Journal of Solid Mechanics Vol. 7, No. 2 (2015) pp. 146-157

# An Experimental and Numerical Study of Forming Limit Diagram of Low Carbon Steel Sheets

M. Kadkhodayan *, H. Aleyasin

*Department of Mechanical Engineering ,Islamic Azad University, Mashhad Branch, Mashhad, Iran*

Received 18 February 2015; accepted 5 April 2015

**ABSTRACT**

The forming limit diagram (FLD) is probably the most common representation of sheet metal formability and can be defined as the locus of the principal planar strains where failure is most likely to occur. Low carbon steel sheets have many applications in industries, especially in automotive parts, therefore it is necessary to study the formability of these steel sheets. In this paper, FLDs, were determined experimentally for two grades of low carbon steel sheets using out-of-plane (dome) formability test. The effect of different parameters such as work hardening exponent ($n$), anisotropy ($r$) and thickness on these diagrams were studied. In addition, the out-of-plane stretching test with hemispherical punch was simulated by finite element software Abaqus. The limit strains occurred with localized necking were specified by tracing the thickness strain and its first and second derivatives versus time at the thinnest element. Good agreement was achieved between the predicted data and the experimental data.



**Keywords :** Forming limit diagram; Out-of-plane; Localized necking; Finite element.



## 1 INTRODUCTION

THE forming limit diagram (FLD) is a useful measure to evaluate the formability of sheet metal. The formability analysis requires to determine whether the amount of deformation exceeds the forming limit at any point in the formed part or not. The formability limit of sheet metal is usually determined by the initiation of localized necking that precedes fracture. FLDs are plots of the major and minor principal strains which can be sustained by sheet materials prior to the onset of localized necking. The principal strains components at necking ($\varepsilon_1, \varepsilon_2$) are determined along the loading paths that range from uniaxial to biaxial, and a locus in strain space is obtained. This locus represents the limit of formability for the as-received sheet under monotonic or proportional loading paths. The most realistic and general method was introduced at the beginning of the 1960s by Keeler and Backofen and Goodwin [6] who proposed the concept of FLD.

The determination of FLDs is a complex task, and researches on FLDs are still the subject of extensive experimental, theoretical and numerical studies. It is known that two types of experimental tests are used to determine the FLD, i.e. the out-of-plane and Marciniak in-plane formability tests. In the Marciniak in-plane test, a sheet metal sample is stretched over a flat-bottomed punch of a cylindrical cross-section. The other test procedure is the conventional out-of-plane (dome) test where a sheet metal sample is clamped between circular die rings and is deformed by a hemispherical punch. The out-of-plane formability test has been used more extensively than the

* Corresponding author.
*E-mail address: kadkhoda@um.ac.ir* (M. Kadkhodayan).

Marciniak in-plane test. From experimental point of view, Hecker [7] and Marciniak–Kuczynski [10] developed experimental techniques to determine out-of-plane and in-plane forming limit diagrams, respectively. Raghavan [15] proposed a simple technique to prepare in-plane specimens for different strain states. By forming a number of sheet specimens with varying widths, different strain states were obtained. The specimens were deformed to fracture and the strain state was evaluated just outside the fracture zone by circle grid method or digital image correlation technique. Finally, by connecting all the limit strain points, the forming limit curve (FLC) was drawn. Experimental determination of a FLD is very time consuming and requires special equipment, which may not always be available.

Moreover, with increase of computational techniques, the numerical predictions of FLDs have become more attractive and the finite element method (FEM) has been selected to simulate the out-of-plane test. By means of FEM, the strains and the stresses in the elements of the sheet metal can be simultaneously calculated in a numerical simulation for each loading step. To analyze the simulation results for the onset of necking, it is essential to establish a failure criterion. To predict the FLD numerically, some procedures have been established for definition of localized neck under various sheet metal forming conditions. Clift et al. [3] used the ductile fracture criterion to predict the forming limits. Based on these criteria, the occurrence of ductile fracture was estimated using the macroscopic stress and strain that occurred during deformation. Yoshida et al. [18] simulated the hemispherical punch-stretching using an elasto-plastic three-dimensional finite element model. Takuda et al. [16] utilized the ductile fracture criteria to predict the forming limit of sheet metal. Ozturk and Lee [12] investigated the application of the ductile fracture criteria for prediction of the FLD of sheet metal. Burn et al. [1] analyzed thinning of sheets to determine the onset of necking by the Nakazima method and constructed the FLDs for whole range of strain ratios. Using the same test, Geiger and Merklein [5] considered that the gradient of major strain changed rapidly when localized necking occurred. Petek et al. [14] put forward a new method for the evaluation of the thickness strain as a function of time as well as the first and second time derivative of the thickness strain. Pepelnjak et al. [13] introduced an alternative method based on the second time derivative of the thickness strain to detect the area of localized necking. They proposed that the maximum of the second temporal derivative of thickness strain corresponded to the onset of necking.

In the recent literatures, efforts to investigate the prediction of localized thinning as functions of material anisotropy have been expanded. Friedman and Pan [4] paid particular attention on the effect of normal plastic anisotropy on limit strains during biaxial sheet stretching. Huang et al. [9] developed a failure prediction methodology by adopting an approximate macroscopic yield criterion for anisotropic porous sheet metals. Cao et al. [2] used a combination of Marciniak-Kuczynski analysis and a general anisotropic yield criterion developed by Karafillis and Boyce. Wu et al. [17] evaluated the anisotropic behavior of some aluminum sheets using the phenomenological approach via some of the recently proposed yield functions.

In the present work, the forming limit diagram of two low carbon steel sheets were evaluated using hemispherical punch and the related features are discussed. A numerical simulation of the out-of-plane with the FE program Abaqus to determine the FLD was carried out and the obtained results were compared with those from the experiment.

## 2 EXPERIMENTAL WORK

### *2.1 Material and equipment*

In this study, the low carbon steel sheets contain ST14 with thickness of 0.7 mm and ST12 with thicknesses of 0.7 mm, 1 mm and 1.25 mm were utilized for experiment. The mechanical properties of steel sheets were obtained by tensile testing machine (Instron) with a maximum tensile force capacity of 5 kN. The specimens were tested along three directions containing parallel ($0^o$), diagonal ($45^o$) and perpendicular ($90^o$) to the rolling direction of the sheet. The standard tensile properties namely, 0.2% yield stress (YS), ultimate tensile stress (UTS), total elongation and strain hardening exponent ($n$) and the plastic strain ratio ($r$) were determined from the load–elongation data obtained from these tests and shown in Table 1. A constant cross head speed of 0.5 mm. $min^{-1}$ was employed in all cases. The normal anisotropy ($\bar{r}$) was calculated using following equation:

$$\bar{r} = \frac{r_o + 2r_{45} + r_{90}}{4} \tag{1}$$

**Table 1**
Mechanical and formability properties of the materials.

| | Tensile direction | Yield strength (MPa) (0.2%) | Ultimate tensile strength (MPa) | Total elongation(%) | Anisotropy ($r$) | Strain hardening coefficient ($n$) | $n \times r$ |
|---|---|---|---|---|---|---|---|
| ST12 | 0 | 182 | 312 | 38 | 1.73 | 0.217 | 0.375 |
| | 45 | 190 | 318 | 37 | 1.54 | 0.201 | 0.309 |
| | 90 | 185 | 319 | 37 | 1.88 | 0.209 | 0.392 |
| | Average | 185.66 | 316.33 | 37.33 | 1.67 | 0.209 | 0.346 |
| ST14 | 0 | 145 | 300 | 42 | 1.87 | 0.233 | 0.435 |
| | 45 | 158 | 307 | 36 | 1.65 | 0.221 | 0.364 |
| | 90 | 154 | 297 | 40 | 2.14 | 0.232 | 0.496 |
| | Average | 152.33 | 301.33 | 39.33 | 1.82 | 0.228 | 0.414 |

*2.2 Test procedure*

In this work, various strain states (including negative and positive minor strain ratios) were generated using Hecker's simplified technique. In this method, the experimental procedure mainly involve three stages containing grid marking of the sheet specimens, punch-stretching of samples to failure (or onset of localized necking) and measurement of strains. By taking different sample geometries all possible strain states in the left-hand and right-hand sides of an experimental FLD were calculated, see Fig. 1. The material blanks were cut in the required direction in the length of 200 mm and in the widths of 25, 50, 75, 100, 125, 150, 175 and 200 mm. The blanks with the widths of 25, 50, 75 and 100 mm had an hourglass shape, which was required for narrow blanks to prevent failure occurred at the blank-holder. A circle-grid pattern with a diameter of 2.5 mm was electro-chemically etched on the surface of all specimens. Forming up to fracture was carried out for each sample on single action hydraulic press of capacity 500 kN using standard die and punch as shown in Fig. 2. A schematic view of die and press is shown in Fig. 3. To prevent any drawing-in during testing of sheet, a binder force of 100 kN was applied. In this experimental technique, the test specimens were clamped between the upper and lower dies through closing the five bolts and the specimens were pushed on the die surface by blank-holder force. A constant punch displacement speed of 5 mm.min$^{-1}$ was used to deform each test specimen. The specimens were deformed until the first crack initiated on the sample, which can be seen visually or directly from the display of punch force on the force gage of hydraulic press.

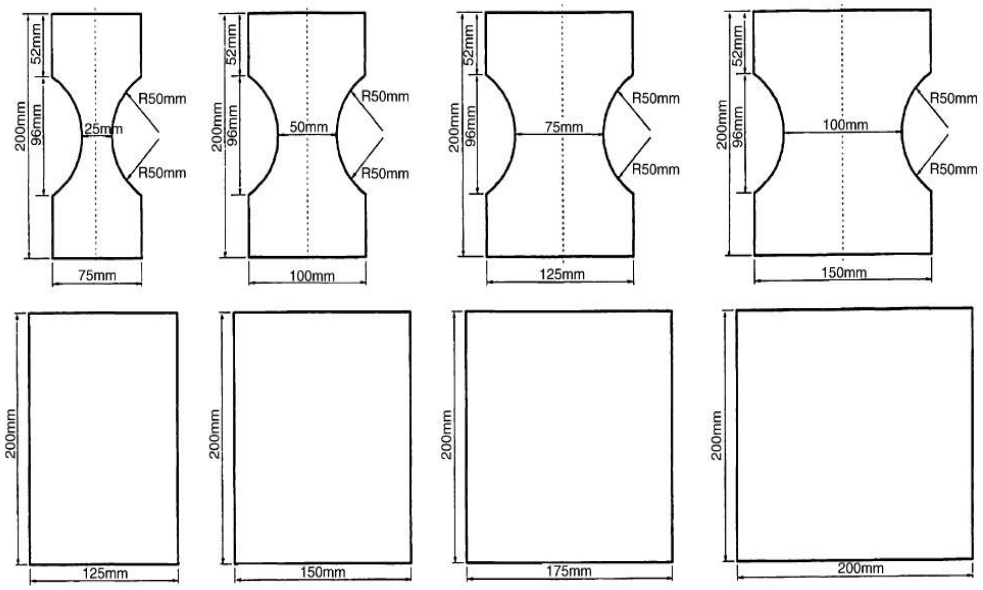


**Fig.1**
The specimens for out-of-plane stretching test.

For each blank width, at least three specimens were tested to obtain more number of data points. Fig. 4 shows the failure positions in the tested specimens. The sheet samples were subjected to different states of strain namely tension–tension, plane strain and tension-compression by varying the width of the samples. During forming, the circles became ellipses of different sizes. The major and minor diameters of the ellipses were measured with an accuracy of 0.01 mm using the megapixel camera as shown in Fig. 5 when the camera was exactly placed vertical and straight in front of the crack of the specimen.

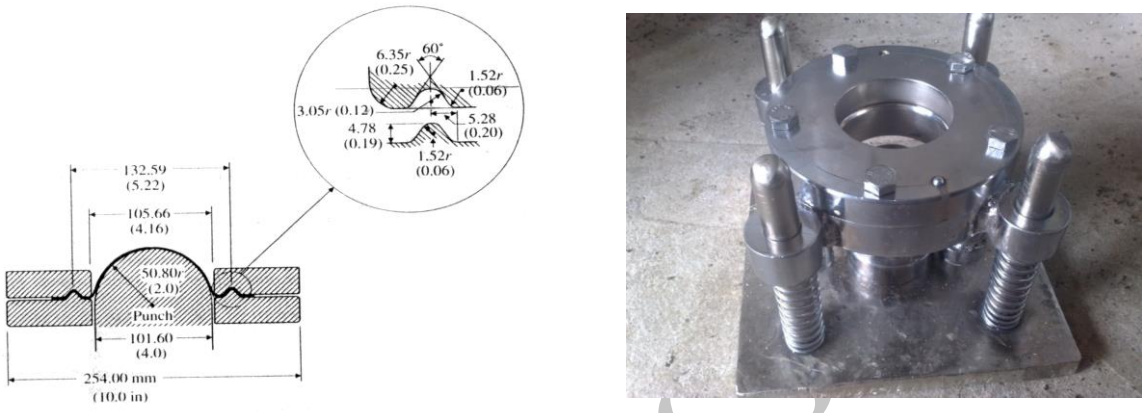


**Fig.2**
Schematic diagram for tooling geometry and the dimensions of the out-of-plane FLD tests.

Major and minor strains, $e_1$ , $e_2$, were calculated in three distinct regions namely safe, necked and fractured regions for all blanks. Finally, the empirical FLDs were drawn by plotting the minor strain along the abscissa and the corresponding major strain along the ordinate. A curve which separates the safe from the unsafe regions can now be drawn, see Fig. 6.

**Fig.3**
A schematic view of the die and the hydraulic press.

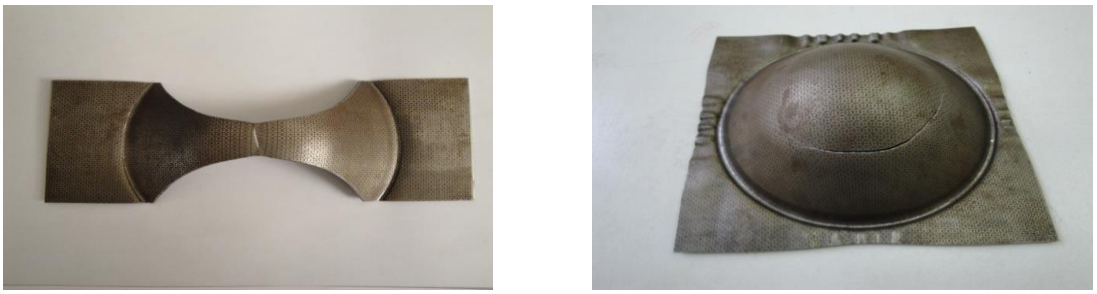

**Fig.4**
Sample stamped specimens used for FLD determination with fracture after testing.

**Fig.5**
Strain measurement equipments.

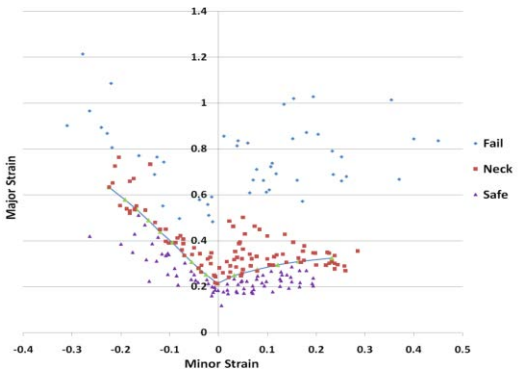


(a)

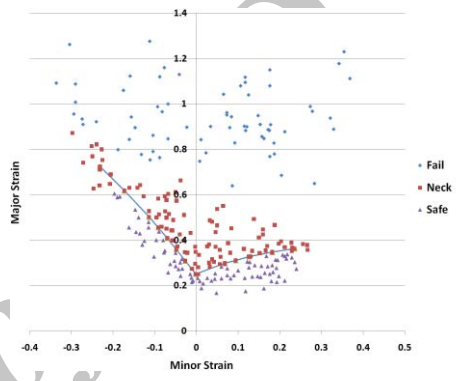


(b)

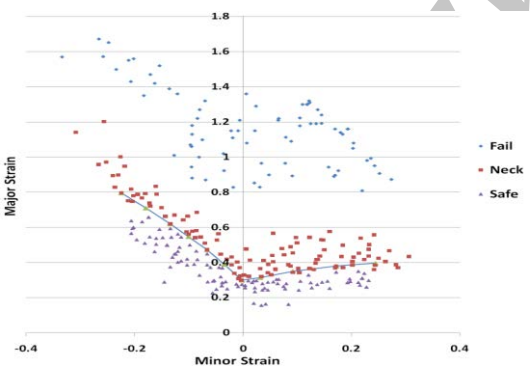


(c)

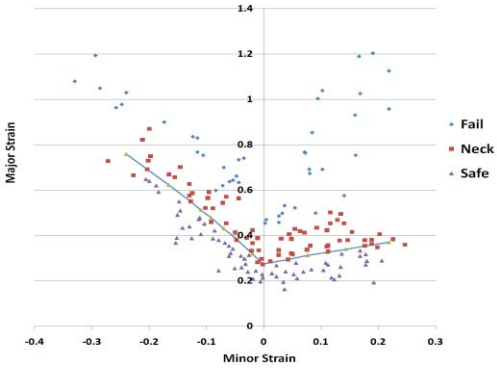


(d)

**Fig.6**
The experimental FLDs for sample sheets: (a) St12-0.7 mm, (b) St12-1 mm, (c) St12-1.25 mm, (d) St14- 0.7 mm .

## 3 FINITE ELEMENT SIMULATION

In this part, the out-of-plane test is analyzed numerically by commercially available code Abaqus to study the formability of the sheet metal. The FE model for the out-of-plane test was composed of a rigid hemispherical punch, an upper die, a lower die with draw bead and a deformable sheet as shown Fig. 2. The material was modeled

as elastic–plastic where the elasticity was taken to be isotropic and the plasticity was assumed as both isotropic and anisotropic conditions. The elasticity of the specimen was defined with a Young's modulus 200 GPa and a Poisson's ratio of 0.3. Due to symmetrical boundary conditions, only one quarter of the entire model was simulated. The S4R element was used in the mesh module. In order to capture the strain localization, the mesh must be sufficiently small and regular. To increase the accuracy, the mesh size in the contact area under the punch was finer than the other parts.

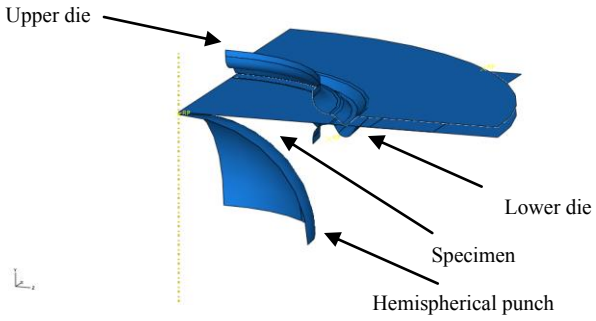


**Fig.7**
FE model of out-of-plane test.

The schematic of the FE model of out-of-plane test setup is shown in Figure 7 with a diameter of hemispherical punch as 100 mm. The contact interaction was modeled by coulomb's law, i.e. the friction coefficients for the punch-blank and die-blank were taken as 0.16 and 0.05, respectively. To take care of the convergence problem, the explicit solver was used. Because in the explicit solver the stability condition is checked for the assurance of the real converged values, the internal energy and kinetic energy curves are presented to prove it as shown in Fig. 8. The simulation process was performed in the two steps. In the first step, the upper die moved down vertically and deformed the sheet into draw bead with a 100 kN force to prevent the specimen sliding between the upper die and the lower die. The hemispherical punch and the lower die stayed fixed during this step. In the second step, while the boundary conditions from the first step were still in effect, the punch started to move up until the desired displacement was achieved.

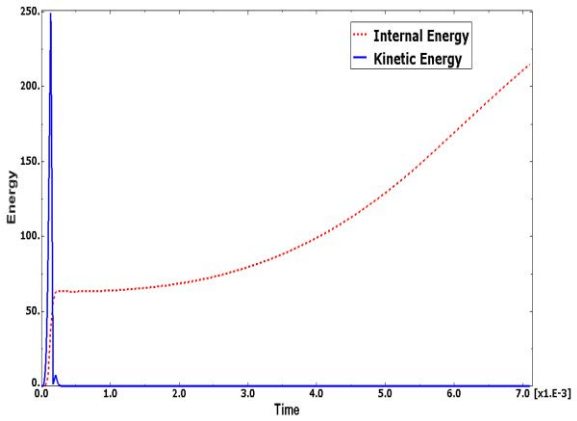


**Fig.8**
Internal energy and kinetic energy as a function of time for blank st12, thickness 1 mm and 200 × 100 mm .

The Hill yield criterion was adopted (Hill, [8]) which can be expressed as:

$$f(\sigma)=\sqrt{F(\sigma_{22}-\sigma_{33})^2+G(\sigma_{33}-\sigma_{11})^2+H(\sigma_{11}-\sigma_{22})^2+2l\sigma_{13}^{\ 2}+2M\sigma_{31}^{\ 2}+2N\sigma_{12}^{\ 2}} \quad (2)$$

where $\sigma_{ij}$ denotes the stress components and $F$, $G$, $H$, $L$, $M$ and $N$ are material constants obtained by tensile tests of the material in the different directions. These constants can be expressed in terms of six yield stress ratios $R_{11}$, $R_{22}$, $R_{33}$, $R_{12}$, $R_{13}$ and $R_{23}$ according to the following relations:

$$\begin{cases} F = \frac{1}{2}\left(\frac{1}{R_{22}^2}+\frac{1}{R_{33}^2}+\frac{1}{R_{11}^2}\right) \\ G = \frac{1}{2}\left(\frac{1}{R_{33}^2}+\frac{1}{R_{11}^2}-\frac{1}{R_{22}^2}\right) \\ H = \frac{1}{2}\left(\frac{1}{R_{11}^2}+\frac{1}{R_{22}^2}-\frac{1}{R_{33}^2}\right) \\ L = \frac{3}{2R_{23}^2} \quad , \qquad M = \frac{3}{2R_{31}^2} \quad , \qquad L = \frac{3}{2R_{12}^2} \end{cases} \tag{3}$$

The anisotropic material data are defined as:

$$\begin{cases} R_{11} = R_{13} = R_{23} = 1 \\ R_{22} = \sqrt{\frac{R_{90}(R_0+1)}{R_0(R_{90}+1)}} \\ R_{33} = \sqrt{\frac{R_{90}(R_0+1)}{R_0+R_{90}}} \\ R_{12} = \sqrt{\frac{3(R_0+1)R_{90}}{2(R_{45}+1)(R_0+R_{90})}} \end{cases} \tag{4}$$

where $R_0$, $R_{45}$ and $R_{90}$ are the plastic strain ratios in different directions relative to the rolling direction, see Table 1.

Fig. 9 shows the effective plastic strains at the onset of necking. As it can be seen the strain localization zones are clearly visible, however, the evaluation of the limit strains is not completely unambiguous.

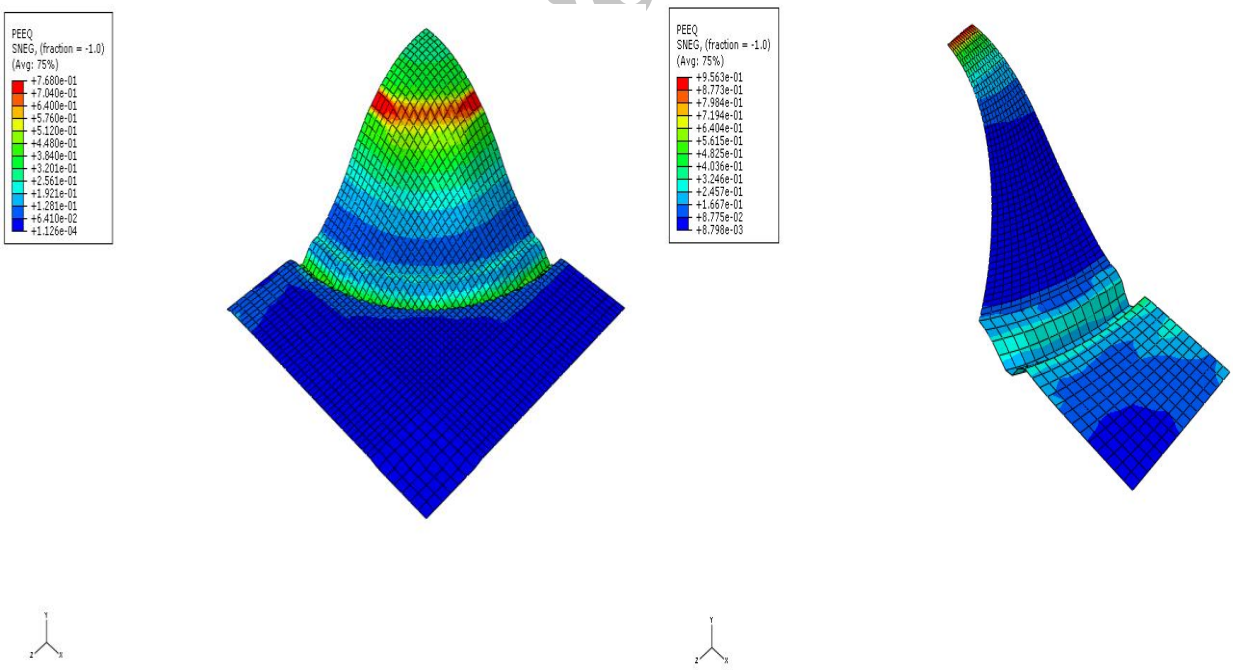


**Fig.9**
Plastic strain distribution of the square and notched specimens.

In order to choose an appropriate criterion to detect the necking, the localized necking was specified by tracing the thickness strain and its first and second derivatives versus time at the thinnest node (Petek, [14] and Pepelnjak, [13]). Fig. 10 shows the thickness strain versus deformation time and its derivatives for a particular element. When necking appears, a sharp change in the strain behavior of the selected element occurs and a knee can be observed on the curve. Thus, considering the thickness strain rate versus time, the first temporal derivative of strain has a maximum. Moreover, the second derivative of thickness strain versus time represents a peak which shows the onset of necking in the specimen, see Fig. 10. In addition, when the load-deflection curve is drawn, a sharp decrease may be observed on the curve which occurs with the peak of the second derivative of thickness strain, simultaneously, which is another criterion to detect the onset of necking. The limit strains were determined by evaluating the main strain states for the selected element at the onset of necking as shown in Fig. 11. To obtain the entire FLD, different specimen geometries were simulated and the main strain states were analyzed for the critical elements. Fig. 12 shows the FLDs obtained from the numerical simulation for the low carbon steel sheet (ST14) with the thickness of 0.7 mm and the low carbon steel sheet (ST12) with the thicknesses of 0.7 mm, 1 mm and 1.25 mm. The predicted FLDs have been compared with the experimental data.

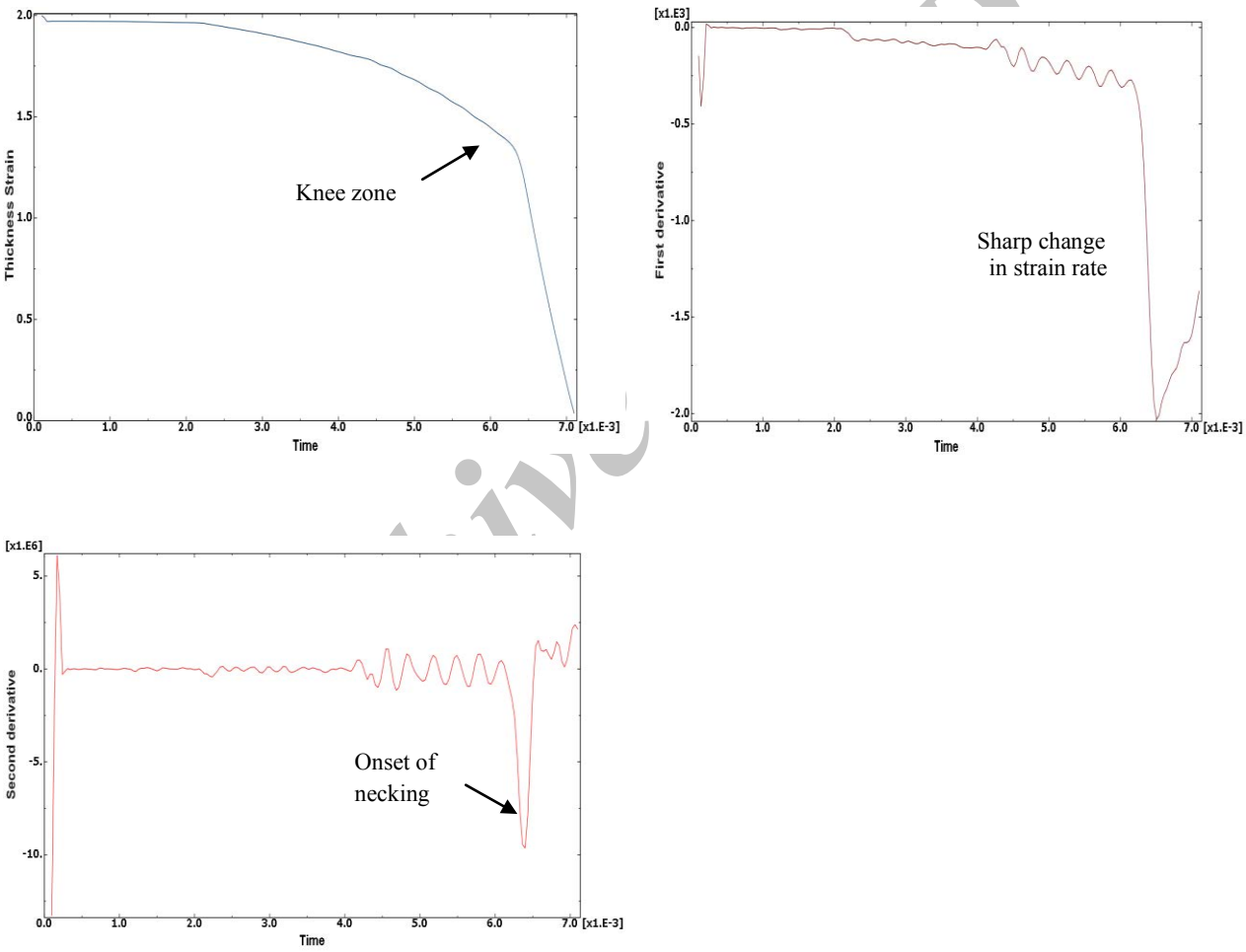


**Fig.10**
Thickness strain as a function of time and its derivatives for a particular specimen.

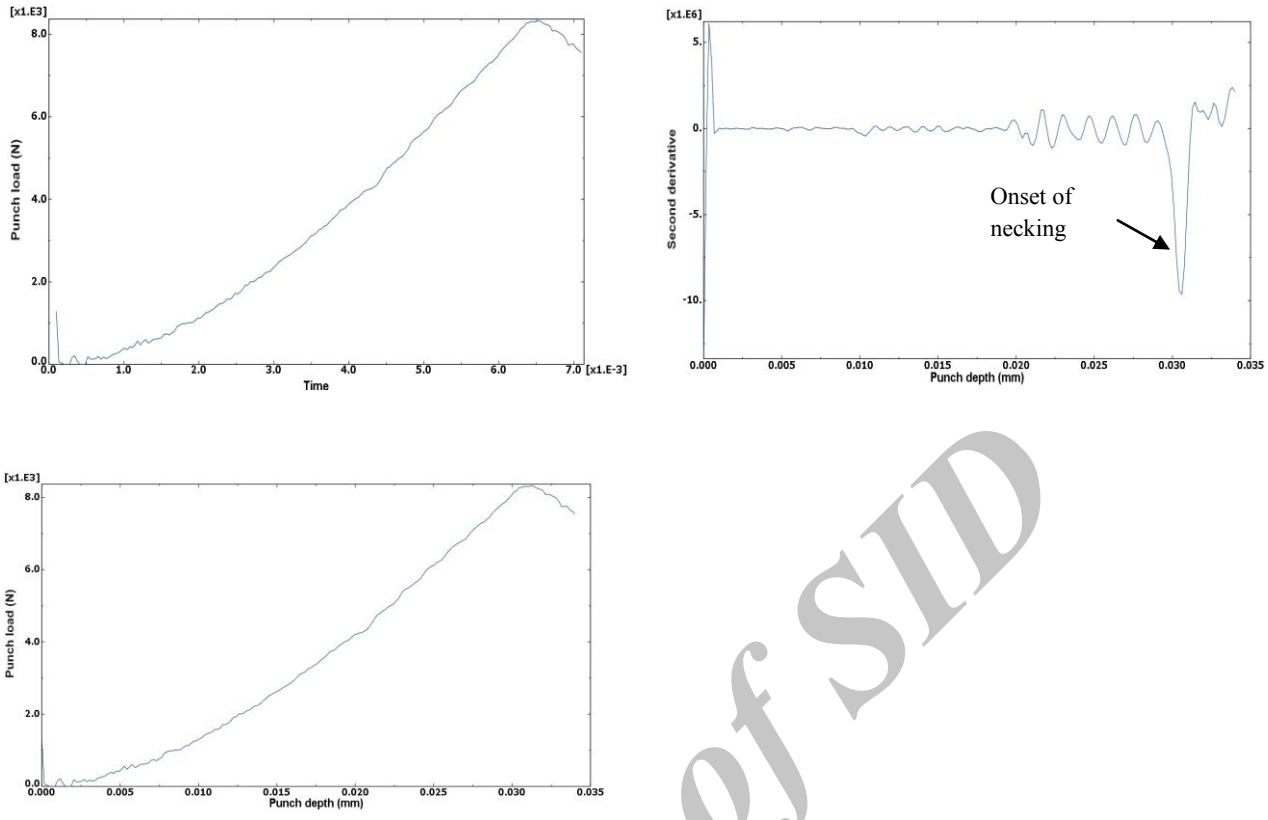


**Fig.11**
Thickness strain as a function of time and its derivatives for a particular specimen.

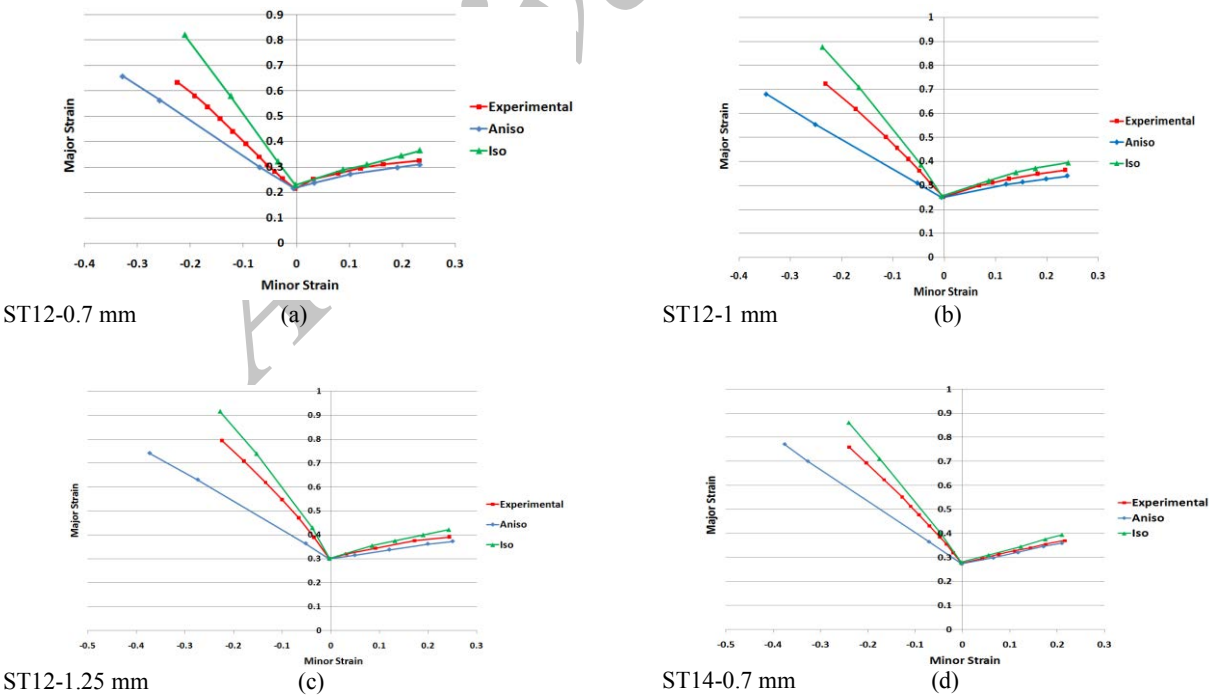


ST12-0.7 mm (a) ST12-1 mm (b)

ST12-1.25 mm (c) ST14-0.7 mm (d)

**Fig.12**
The experimental and numerical FLDs.

## 4 RESULTS AND DISCUSSION

### *4.1 Influence of r and n values*

A comparison between the experimental forming limit curves for ST12 and ST14 steel sheets with thickness of 0.7 mm are shown in Fig. 13. In general, the strain-hardening exponent and the plastic strain ratio of a material can be considered as the most important parameters which affect on the FLD. According to Fig. 13, the forming limit curve for ST14 steel sheet has more limiting strains than ST12. By increasing the strain-hardening exponent ($n$), the forming limit curves are shifted upward. The strain-hardening exponent generally delays the onset of instability until the higher strain value is reached.

The plastic anisotropy rises due to the preferred orientation of grains in a polycrystalline material which is usually characterized by the $r$ value. It is usually known that the high plastic stain ratio or normal anisotropy is useful to improve the draw-ability (tension-compression strain condition), because it causes good resistance to thinning in the thickness direction during deep drawing.

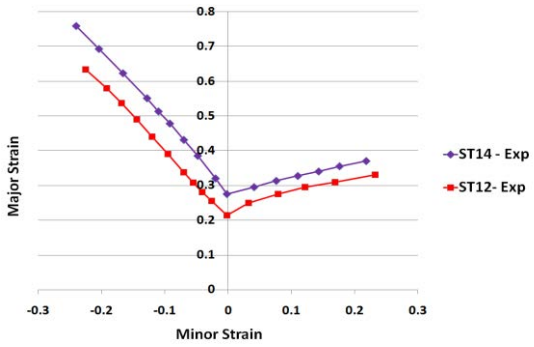


**Fig.13**
The experimental forming limit curves of ST12 and ST14 steel sheets with thickness of 0.7 mm.

In the current study, the ST14 steel sheet has higher value of normal anisotropy, $\bar{r}$, than ST12 steel sheet, see Table 1. This means that ST14 steel sheet of thickness 0.7 mm shows higher draw-ability than ST12 with the same thickness. According to Fig. 13, the difference between the FLDs in the tension-tension strain condition (stretch ability) is less than that of the tension-compression part. In other words, the effect of normal anisotropy in the left-hand side is more than that in the right-hand side which verifies what is known as the better formability of the tension–compression region. Furthermore, the average value of $n \times r$ represents the stretch-ability of a material so that the higher amount of $n \times r$ shows more stretch-ability (Narayanasamy and Sathiya Narayanan, [11]). Table 1. shows that the average value of $n \times r$ for ST14 steel sheet is more than that for the ST12 which shows the better stretch-ability of ST14 steel for the same thickness, see Fig. 13.

### *4.2 Influence of sheet thickness*

Fig. 14 shows the different FLDs obtained from the experimental results for the low carbon steel sheets ST12 with three thicknesses of 0.7 mm, 1mm and 1.25mm. It is visible that the steel sheet of thickness 1.25 mm exhibits better stretch-ability and draw-ability than that of other two thicknesses. For instance, the sheets with thicknesses of 0.7 mm, 1 mm and 1.25 mm at a maximum minor strain of 0.23 in tension-tension region possesses maximum major strains of 0.325, 0.364 and 0.396, respectively. In tension-compression strain condition, the maximum minor strain offered by ST12 steel sheet of three mentioned thicknesses is about 0.225. Whereas the maximum major strain offered by the sheets with thicknesses of 0.7 mm, 1 mm and 1.25 mm are 0.634, .725 and 0.796, respectively. It is found that the maximum major strain offered by the sheet of thickness 1.25 mm in tension-compression region is more than twice of that for the sheet of thickness 0.7 mm in tension-tension region. Therefore, increasing the thickness of the sheets in tension-compression region can enhance its formability because the sheet can accommodate more amount of plastic deformation compared with that in the tension-tension region (Narayanasamy and Sathiya Narayanan, [11]). The FLDs of ST12 steel of thickness 1.25 mm and of ST14 steel of thickness 0.7 mm obtained from the experimental result are given in the Fig. 6(c) and 6(d), respectively.

The ST14 with the thickness of 0.7 mm has the maximum minor strain of 0.218 while for the ST12 with the thickness of 1.25 it is 0.244 in tension-tension region. Moreover, the maximum major strain offered by ST14 with the thickness of 0.7 mm is 0.370 while it is 0.391 for the ST12 steel with the thickness of 1.25 mm. It shows that the thickness effect can be compensated somehow by the material change. In plane strain condition, the limiting major

strain offered by ST14 steel sheet of thickness 0.7 mm is about 0.275 while it is about 0.3 for the ST12. In tension-compression strain condition, the maximum minor strain offered by ST14 steel sheet of thickness 0.7 mm is 0.24, but it is 0.224 for the ST12 with thickness 1.25 mm. Whereas the maximum major strain offered by ST14 steel sheet of thickness 0.7 mm is 0.759 and for the ST12 of thickness 1.25 mm it is 0.796.

By comparing the above results, it can be concluded that the effect of strain-hardening exponent and plastic anisotropy are more significant than thickness in increasing the formability, i.e. the FLD of ST14 with higher strain-hardening exponent and plastic anisotropy than ST12, is between the FLDs for ST12 with thickness of 1 mm and 1.25 mm.

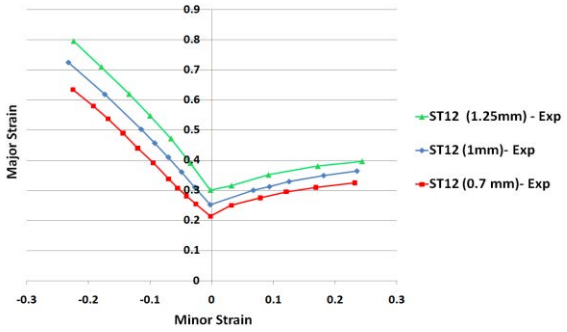


**Fig.14**
Effect of thickness on the FLD of ST12 steel sheet.

*4.3 Prediction of limit strain by FE simulation*

The results obtained from the FE simulation using Abaqus software are in good agreement with the experimental data, see Fig. 12. The Exp, Iso and Aniso stand for the experimental and modeling data for isotropic and anisotropic conditions, respectively. In isotropic condition, the FLDs are determined at the right- and left-hand sides have higher values of limit major strains than the experimental FLDs but the anisotropic simulated curves are under the experimental curves. This shows that in the equal strain-hardening exponent, the isotropic condition exhibit better formability than the anisotropic condition.

On the right-hand side, the forming limit curves obtained from numerical simulations are consistent with the experimental results more precisely for both isotropic and anisotropic conditions. However, the simulated curves for isotropic state have more tendency toward experimental curves. As shown in Fig. 12, the simulated results show greater formability in isotropic state for thicker sheets. On the right-hand side, the anisotropic curve of ST14 sheet with thickness of 0.7 mm has the best fit with the experimental results, see Fig. 12(d). On the other hand, the isotropic curves predict higher draw-ability than anisotropic and experimental ones, while the experimental data are placed between them. The differences between curves are more significant in the left-hand side of FLDs.

On the left-hand side of FLDs and for the anisotropic conditions, as thickness decreases the simulation curves approach to the experimental curves. But for the isotropic conditions, with increasing the thickness of the sheet, the slope of the simulation curves decrease and the curves approach the experimental curves. This trend of numerical results could be attributed to the inaccurate estimation of normal anisotropy for the anisotropic condition. While for the isotropic conditions which contain more approximate assumptions different trend are observed, Fig. 12. Moreover, it is seen that in both left- and right-regions of the FLDs, the anisotropic simulated curves have lower values of the major strains than the experimental curves which shows their more reliability for the practical application.

Another important parameter in the forming limit curve is the principal strain known as $FLD_O$, which is equal to the major principal strain at failure when the minor principal strain is zero. According to Fig. 12, the forming limit strains in the plain-strain state, $FLD_O$ are predicted by both isotropic and anisotropic conditions are in good agreement with the experimental results for all sheets. However, the ST14 sheet has a higher value of $FLD_O$ than the ST12 sheet for the same thickness of 0.7 mm. This difference can be attributed to the difference of $n \times r$ for these two cases which are 0.414 and 0.346, respectively. In addition, the ST12 sheet with thickness of 1.25 mm has higher value of $FLD_O$ than those of the sheets with less thicknesses which is due to its formability properties, i.e. more thicker plate has more limit stain values.

## 5 CONCLUSIONS

The formability of low carbon steel sheets was investigated by experimental and numerical approaches. The effect of strain-hardening exponent ($n$) and plastic strain ratio ($r$-value) along with the effect of thickness on FLDs were observed. To carry out the experiment, the out-of-plane test procedure was used to determine the complete forming limit curve for sheet metal. The experimental results showed that by increasing the values of strain-hardening exponent ($n$) and plastic anisotropy ($r$-value), the formability of the sheet increased. Moreover, the steel sheet with higher values of normal anisotropy had more draw-ability. In addition, by increasing the thickness of the sheet, the forming limit strain increased. It was found that the effect of strain-hardening exponent and plastic anisotropy are more significant than thickness in increasing the formability. The out-of-plane stretching test was simulated by FE software Abaqus and the localized necking of low carbon steel sheets was predicted by tracing the thickness strain and its first and second derivatives versus time at the thinnest nodes for different specimens. The numerically obtained forming limit curves are in good agreement with the experimental results.

## REFERENCES


[1] Brun R., Chambard A., Lai M., De Luca P., 1999, Actual and virtual testing techniques for a numerical definition of materials, *Numisheet 99*.

[2] Cao J., Yao H., Karafillis A., Boyce M.C., 2000, Prediction of localized thinning in sheet metal using a general anisotropic yield criterion, *International Journal of Plasticity* **16**: 1105-1129.

[3] Clift S.E., Hartley P., Sturgess C.E.N., Rowe G.W., 1990, Fracture prediction in plastic deformation processes, *International Journal of Mechanical Sciences* **32**: 1-17.

[4] Friedman P.A., Pan J., 2000, Effects of plastic anisotropy and yield criteria on prediction of forming limit curves, *International Journal of Mechanical Sciences* **42**: 29-48.

[5] Geiger M., Merklein M., 2003, Determination of forming limit diagrams- a new analysis method for characterization of materials formability, *Annals of the CIRP* **52**: 213-216.

[6] Goodwin G.M., 1968, Application of strain analysis to sheet metal forming problems in the press shop, *SAE Technical Paper 680093*, doi:10.4271/680093.

[7] Hecker S.S., 1975, Simple technique for determining forming limit curves, *Sheetmetal Industries Ltd* **52**: 671-676.

[8] Hill R., 1948, A theory of yielding and plastic flow of anisotropic metals, *Proceedings A* **193**: 281-297.

[9] Huang H.M., Pan J., Tang S.C., 2000, Failure prediction in anisotropic sheet metals under forming operations with consideration of rotating principal stretch directions, *International Journal of Plasticity* **16**: 611-633.

[10] Marciniak Z., Kuczynski K., 1967, Limit strains in the processes of stretch forming sheet metal, *International Journal of Mechanical Sciences* **9**: 609-620.

[11] Narayanasamy R., Sathiya Narayanan C., 2006, Forming limit diagram for Indian interstitial free steels, *Materials & Design Journal* **27**: 882-899.

[12] Ozturk F., Lee D., 2004, Analysis of forming limits using ductile fracture criteria, *Journal of Materials Processing Technology* **147**: 397-404.

[13] Pepelnjak T., Petek A., Kuzman K., 2005, Analysis of the forming limit diagram in digital environment, *Advanced Material Research* **6/8**: 697-704.

[14] Petek A., Pepelnjak T., Kuzman K., 2005, An improved method for determining a forming limit diagram in the digital environment, *Journal of Mechanical Engineering* **51**: 330-345.

[15] Raghavan K.S., 1995, A simple technique to generate in-plane forming limit curves and selected applications, *Metallurgical and Materials Transactions A* **26**(8): 2075-2084.

[16] Takuda H., Mori K., Takakura N., Yamaguchi K., 2000, Finite element analysis of limit strains in biaxial stretching of sheet metals allowing for ductile fracture, *International Journal of Mechanical Sciences* **42**: 785-798.

[17] Wu P.D., Jain M., Savoie J., MacEwen S.R., Tugcu P, Neale K.W., 2003, Evaluation of anisotropic yield functions for aluminum sheets, *International Journal of Plasticity* **19**: 121-138.

[18] Yoshida T., Katayama T., Usuda M., 1995, Forming-limit analysis of hemispherical-punch stretching using the three-dimensional finite element method, *Journal of Materials Processing Technology* **50**: 226-237.